European Radiology (2019) 29:2233–2242
https://doi.org/10.1007/s00330-018-5865-5

COMPUTED TOMOGRAPHY

Diabetes risk assessment with imaging: a radiomics study of abdominal CT

Chun-Qiang Lu[1] · Yuan-Cheng Wang[1] · Xiang-Pan Meng[1] · Hai-Tong Zhao[2] · Chu-Hui Zeng[1] · Weiwei Xu[1] · Ya-Ting Gao[1] · Shenghong Ju[1]

Received: 11 June 2018 / Revised: 9 October 2018 / Accepted: 25 October 2018 / Published online: 6 December 2018

Abstract

Objectives To identify CT markers for screening of early type 2 diabetes and assessment of the risk of incident diabetes using a radiomics method.

Methods The medical records of 26,947 inpatients were reviewed. A total of 690 patients were selected and allocated to a primary cohort, a validation cohort, and a prediction cohort and used to build prediction models for diabetes. Three radiomics signatures were constructed using CT image features extracted from three regions of interest, i.e., in the pancreas, liver, and psoas major muscle. By incorporating radiomics signatures and other markers, we built a radiomics nomogram that could be used to screen for early diabetes and predict future diabetes.

Results Of the three abdominal organs for which radiomics signature were constructed, that of the pancreas showed the best discriminatory power for early diabetes screening and prediction (C-statistics of 0.833, 0.846, and 0.899 for the primary cohort, validation cohort, and prediction cohort, respectively). The sensitivity and specificity of the nomogram for prediction of 3-year incident diabetes were 0.827 and 0.807, respectively.

Conclusions This study presents alternative radiomics markers that have potential for use in screening for undiagnosed type 2 diabetes and prediction of 3-year incident diabetes.

Key Points

- *CT images may provide useful information to evaluate the risk of developing diabetes.*
- *Radiomics score for diabetes prediction is based on subtle changes of abdominal organs detected by CT.*
- *The radiomics signature of pancreas, a combination of five features of CT images, is efficient for early diabetes screening and prediction of future diabetes (AUC > 0.8).*

Keywords Diabetes mellitus · Multidetector computed tomography · Pancreas · Adipose tissue

Abbreviations

AAT	Abdominal adipose tissue
CI	Confidence interval
CT	Computed tomography
LASSO	Least absolute shrinkage and selection operator
MRI	Magnetic resonance imaging
ROC	Receiver-operating characteristic
ROI	Region of interest
SAT	Subcutaneous adipose tissue
VAT	Visceral adipose tissue

Electronic supplementary material The online version of this article (https://doi.org/10.1007/s00330-018-5865-5) contains supplementary material, which is available to authorized users.

✉ Shenghong Ju
jsh0836@hotmail.com

[1] Jiangsu Key Laboratory of Molecular and Functional Imaging, Department of Radiology, Zhongda Hospital, Medical School of Southeast University, 87 Ding Jia Qiao Road, Nanjing 210009, China

[2] Lab of Image and Signal Processing, School of Biological Science and Medical Engineering, Southeast University, Nanjing, China

Introduction

The complications of diabetes have led to significant increases in the morbidity associated with the disease [1, 2]. Lifestyle changes and timely medical intervention are thought to be the most effective ways of reducing the risk [3]. Recent studies

have demonstrated a high proportion of undiagnosed diabetes worldwide [4–6]. Moreover, the current methods used to diagnose type 2 diabetes, such as the oral glucose tolerance test and hemoglobin A_{1C} level measurement, may not be satisfactory for mass screening [7]. Therefore, there is a need to develop new methods for both early detection and risk assessment of the disease. However, although a number of studies have assessed the ability of various measures to predict the development of type 2 diabetes [8–14], the discriminative power of these studies has been limited.

Type 2 diabetes is a metabolic syndrome that starts with insulin resistance [15]. Obesity, especially abdominal obesity, is the major risk factor for insulin resistance [16]. Both visceral (VAT) and subcutaneous (SAT) adipose tissues contribute to abdominal obesity. Previous studies suggested that VAT or VAT/SAT was a unique risk factor for metabolic disease and associated with insulin resistance [17–21]; however, the predictive value still needs more investigation. Furthermore, an abnormality of lipid metabolism manifesting as hyperlipidemia and ectopic lipid deposition in the abdominal organs occurs before the onset of type 2 diabetes [22] and is closely related to insulin resistance and islet β cell dysfunction [23]. Therefore, direct detection of structural changes, such as lipid deposition in target abdominal organs, could be an effective approach for acquiring important information when evaluating the risk of diabetes.

Pathological changes in the abdominal organs can be evaluated by radiological methods, such as CT and MRI [24]. The radiomics method is expected to overcome the limitation of visual assessment of images that provide little information about histogram and texture features in a region of interest (ROI) [25–27]. This technique has had considerable success for the diagnosis and assessment of tumors [28–30].

Therefore, it is reasonable to hypothesize that the pathological structural alterations in the abdominal organs related to incident diabetes could be detected using new radiological methods. Similarly, findings on medical imaging might also provide information on the risk of developing diabetes. The aim of this study was to identify imaging markers and develop a model for both diagnosis of early diabetes and prediction of future diabetes by combining abdominal CT images and radiomics methods.

Materials

Ethical approval (No. 2017ZDKYSB086) was obtained from the Institutional Ethics Committee of Zhongda Hospital, Medical School of Southeast University (Nanjing, China), and the requirement for informed consent was waived. All patients enrolled in the study had been hospitalized at our institution.

Subjects

Three groups of patients were enrolled. The first group consisted of patients who were either newly diagnosed with type 2 diabetes or had had this diagnosis for less than 3 years. The second group consisted of control subjects who did not have diabetes and had normal blood glucose levels. The third group was an additional prediction group that consisted of patients who did not have diabetes and had normal blood glucose levels but were diagnosed with type 2 diabetes within 1 to 3 years. Data for the patient inclusion and exclusion criteria (Appendix A1), screening process (Appendix A2), disease composition (Figure S5), and incomplete fasting plasma glucose levels (Appendix A2) are shown in the Supplemental materials.

The study was logically divided into three parts. In the first part, a retrospective case-control study was performed to identify imaging markers for early diabetes. A primary cohort comprising patients with early diabetes and non-diabetic controls was used to develop three radiomics signatures corresponding to the pancreas, liver, and psoas major muscle for classification of early diabetes. An independent validation cohort was used to determine the discrimination performance of these radiomics signatures. The second part was a retrospective cohort study. A prediction cohort comprising pre-diabetic patients (not patients with pre-diabetes, see Appendix A2) and non-diabetic controls was established to perform a second validation to determine whether these radiomics signatures were able to predict future diabetes. Finally, the radiomics signatures were combined with other information to build a nomogram for diagnosis of early diabetes and prediction of future diabetes. Patients who were hospitalized in our institution from January 2007 to November 2013 were enrolled as the primary cohort and those hospitalized from December 2013 to December 2016 were enrolled as the validation cohort. The prediction cohort comprised patients hospitalized from January 2007 to November 2013. The non-diabetic controls were randomly selected and matched with the patients who had early diabetes in the primary cohort in terms of age, sex, and CT scan date using the propensity score matching method [31].

CT image acquisition, retrieval procedure, and radiomics feature extraction methodology

All CT images were retrieved in DICOM format from the institutional archives. Three ROIs were delineated around the pancreas, liver, and psoas major muscle in the slice showing the maximum cross-section (Fig. 1).

A texture analysis was performed on the images of target organs using in-house texture analysis software with algorithms implemented in MATLAB 2012b (Mathworks). In total, 160 imaging features derived from the category of

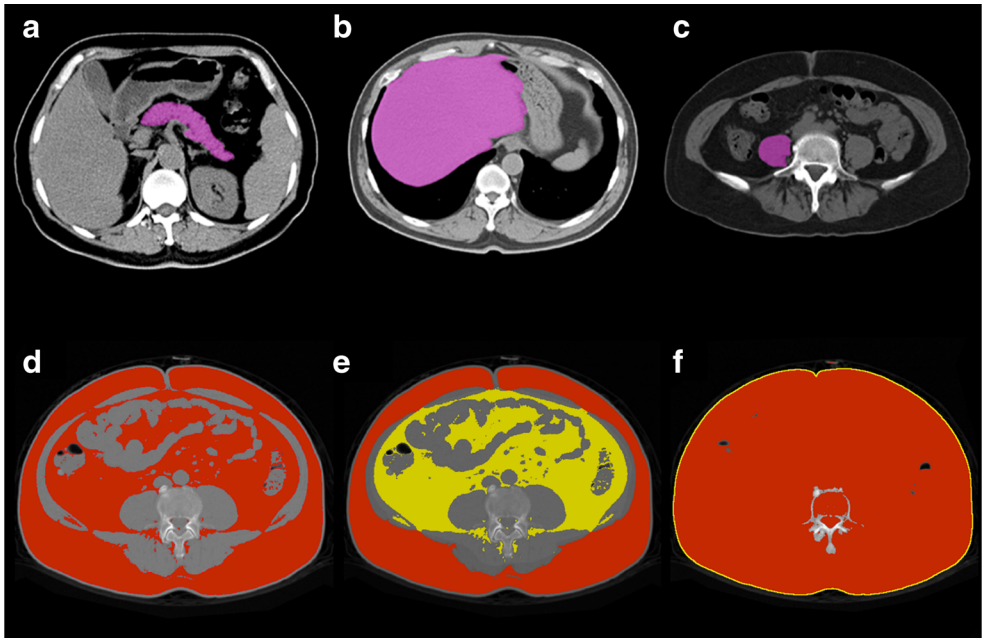

Fig. 1 ROI drawing and fat distribution parameters calculating procedure. Upper panel: representative illustrations of ROI drawing on different abdominal organs. The purple area represents the area of ROI. **a** ROI of pancreas; **b** ROI of the liver; and **c** ROI of psoas major muscle. All the ROIs were delineated by two radiologists (with 5 years and 3 years of experience in abdominal CT images) blinded to the case/control status. Two sets of features extracted from the ROIs delineated by the two radiologists were used to test the stability of the radiomics features. The features extracted from ROIs delineated by the radiologist with 5-year experience were used for further analysis. Focal lesions or abnormal intensity were carefully avoided so as not to be included in the ROI. Bottom panel: representative illustrations of fat distribution parameters and waist circumference. By setting the gray-level threshold between -190 and -30 HU, the adipose tissue was segmented automatically, and the area parameter was measured. The area of SAT and VAT was manually separated and measured by two radiologists with 3-year experience. **d** adipose tissue (red); **e** subcutaneous adipose tissue (red) and visceral adipose tissue (yellow); and **f** waist circumference (length of yellow line)

histogram and the gray-level co-occurrence matrix were extracted from one ROI on the CT image with or without an image filtering process (Laplacian of Gaussian spatial band-pass filter) for each subject. The details concerning the extraction of the imaging features are provided in the Supplemental materials (Appendix A3). Some studies reported that CT imaging parameters including voxel size and slice thickness significantly affect radiomics features extracted using quantitative algorithms [32, 33], so we extracted the imaging parameters and compared them between groups within each of the three cohorts.

Calculation of fat distribution parameters

One abdominal slice located at the level of the L5 vertebra was selected for analysis for each subject. The waist circumference (cm) of each subject was measured on this CT image slice using the ImageJ software. The area of adipose tissue (AAT, cm2), visceral adipose tissue (VAT, cm2), and subcutaneous adipose tissue (SAT, cm2) were measured for each patient also using ImageJ software, and the VAT/SAT ratio was then calculated (Fig. 1).

Selection of features and building the radiomics signatures

The number of CT scans for pre-diabetic patients that met the inclusion criteria was too small for a cross-validation analysis, so we attempted to find an indirect way of building a model for prediction of diabetes. Firstly, we identified radiomics markers and built a logistic regression model for detection of early diabetes and then attempted to determine whether these markers and the model could predict future diabetes.

Least absolute shrinkage and selection operator (LASSO) and 10-fold cross-validation methods were used to reduce the dimensions of the data and to select the most predictive features. All imaging features for the three organs were selected to build three separate LASSO regression models. Three radiomics scores (Rad scores, value of radiomics signature) corresponding to the LASSO analyses were calculated for each patient using a linear combination of selected features that were weighted by their respective coefficients.

The Harrell C-index values (C-statistics) for the Rad scores in the three cohorts were calculated to evaluate the discrimination performance of the three radiomics signatures [34]. A C-index value of 0.5 indicates that the information is of no

Table 1 Characteristics of patients in the primary and validation cohorts

Characteristic	Primary cohort			Validation cohort		
	Diabetes ($n = 198$)	Non-diabetes ($n = 198$)	p value	Diabetes ($n = 95$)	Non-diabetes ($n = 95$)	p value
Age, years	63.67 ± 11.18	63.57 ± 11.16	0.938	65.30 ± 10.32	65.21 ± 10.48	0.945
Sex, *n* (%)			0.919			0.719
Male	118 (59.6)	117 (59.1)		45 (47.4)	43 (45.3)	
Female	80 (40.4)	81 (40.9)		50 (52.6)	52 (54.7)	
Radiomics score						
Pancreas ROI	0.55 (-0.02, 1.27)	-0.58 (-1.16, -0.21)	< 0.001	0.77 (0.29, 1.41)	-0.45 (-1.00, 0.08)	< 0.001
Liver ROI	0.12 (-0.18, 0.57)	-0.22 (-0.63, 0.15)	< 0.001	0.05 (-0.34, 0.62)	-0.38 (-0.77, 0.13)	< 0.001
Psoas major ROI	0.05 (-0.09, 0.18)	-0.08 (-0.20, 0.08)	< 0.001	0.10 (-0.02, 0.26)	-0.05 (-0.17, 0.14)	< 0.001
Waist circumference, cm	94.52 ± 10.68	89.93 ± 11.05	< 0.001	96.59 ± 10.50	89.98 ± 9.78	< 0.001
AAT, cm^2	364.33 ± 129.62	304.50 ± 127.86	< 0.001	391.21 ± 144.98	314.79 ± 112.52	< 0.001
SAT, cm^2	195.18 ± 86.11	162.17 ± 76.55	< 0.001	207.08 ± 98.02	171.04 ± 70.42	0.004
VAT, cm^2	169.16 ± 63.77	142.31 ± 67.82	< 0.001	184.13 ± 71.00	143.75 ± 62.20	< 0.001
VAT/SAT	0.96 ± 0.40	0.96 ± 0.43	0.896	0.99 ± 0.45	0.92 ± 0.40	0.228

The radiomics scores are presented as the median (interquartile range) and the other data are presented as the mean ± standard error of the mean except for the patient sex data. Patient age and sex were balanced using propensity score matching

AAT area of abdominal adipose tissue, *ROI* region of interest, *SAT* area of subcutaneous abdominal adipose tissue, *VAT* area of visceral abdominal adipose tissue, *VAT/SAT* ratio of VAT to SAT

predictive value while a value close to 1 indicates a perfectly predictive information. Finally, the data from the primary cohort, including age, sex, waist circumference, the Rad score for each of the three abdominal organs, and the fat distribution parameters, were used to develop a multivariable logistic regression model and build a radiomics nomogram based on multivariable logistic analysis (Supplemental materials, Appendix A4). The discrimination performance of the nomogram was also validated in the three cohorts.

Statistical analysis

The statistical analysis was conducted using SPSS version 19.0 software (IBM Corp.) and R version 3.0.1 software.

Table 2 Characteristics of patients in the prediction cohort

Characteristic	Prediction cohort		p value
	Patients with pre-diabetes ($n = 52$)	Patients with no diabetes ($n = 52$)	
Age, mean ± SD, years	63.63 ± 11.37	63.17 ± 9.95	0.826
Sex, *n* (%)			0.838
Male	33 (63.5)	34 (65.4)	
Female	19 (36.5)	18 (34.6)	
Radiomics score			
Pancreas ROI	0.47 (0.01, 0.76)	-0.39 (-0.64, -0.12)	< 0.001
Liver ROI	0.01 (-0.11, 0.28)	-0.04 (-0.31, 0.17)	0.145
Psoas major ROI	0.16 (-0.25, 0.67)	-0.24 (-0.60, 0.30)	0.004
Waist circumference, cm	96.38 ± 12.02	91.62 ± 11.78	0.044
AAT, cm^2,	398.12 ± 142.55	326.64 ± 136.58	0.010
SAT, cm^2,	215.88 ± 91.17	180.15 ± 87.08	0.044
VAT, cm^2	182.24 ± 70.23	146.48 ± 71.46	0.012
VAT/SAT	0.90 ± 0.30	0.91 ± 0.38	0.917

The radiomics scores are presented as the median (interquartile range) and the other data are presented as the mean ± standard error of the mean, except for the patient sex data. Age and sex were balanced using propensity score matching

AAT area of abdominal adipose tissue, *ROI* region of interest, *SAT* area of subcutaneous abdominal adipose tissue, *VAT* area of visceral abdominal adipose tissue, *VAT/SAT* ratio of VAT to SAT

The Student's t test or the Mann-Whitney U test was used to compare continuous variables and the χ^2 test was used to compare categorical variables. Two packages (glmnet and rms) in R were used in this study. The reported statistical significance levels are all two-sided, with statistical significance set at 0.05.

Results

Characteristics of patients

Six hundred ninety patients were selected from a total of 26,947 consecutive inpatients in the institutional database. The characteristics of the patients in the three cohorts are shown in Tables 1 and 2. The group with diabetes had a higher waist circumference and larger areas of abdominal adipose tissue (AAT), VAT, and SAT than the non-diabetic controls in all three cohorts (all $p < 0.05$); however, there was no significant difference in the VAT/SAT ratio between the patients with diabetes and the controls. There were differences in some of the CT imaging parameters in the first two cohorts, but not in the prediction cohort (Appendix Tables 2 and 3).

Selection of features and building a radiomics signature

Three LASSO logistic regression models corresponding to the imaging features of the different ROIs were built. The Rad scores for the three ROIs were significantly different between the groups in the primary and validation cohorts (Tables 1 and 2, all $p < 0.001$). The formula used to calculate the Rad score is described in the Supplemental materials (Appendix A5–A7).

Diagnostic validation of the radiomics signature

The radiomics signature built from the features of the ROI in the pancreas yielded a C-index of 0.833 in the primary cohort and 0.846 in the validation cohort (Table 2). The radiomics signature of the ROI in the liver yielded a C-index of 0.697 in the primary cohort and 0.687 in the validation cohort. The radiomics signature of the ROI in the psoas major muscle

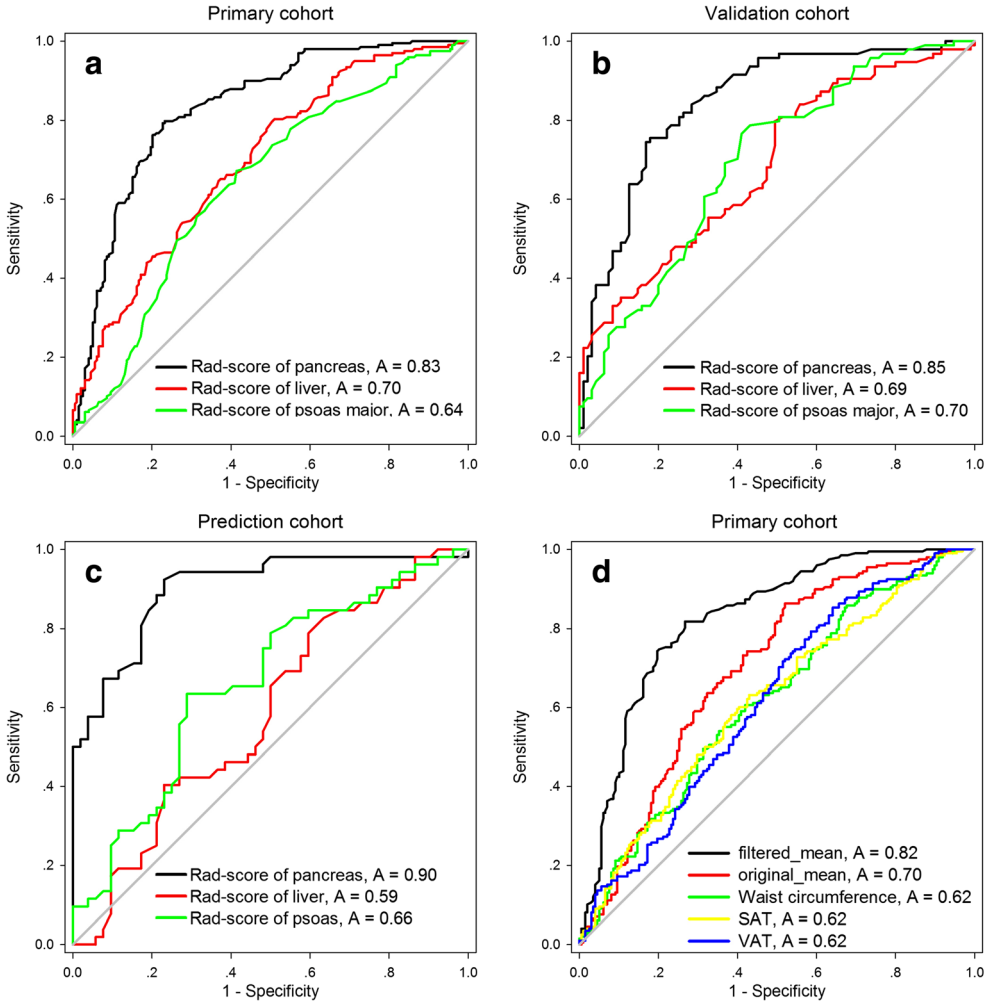

Fig. 2 Receiver-operating characteristic curves for the different parameters in the three cohorts. **a** The AUC for the radiomics signatures of the pancreas, liver, and psoas major in the primary cohort. **b** The AUC for the radiomics signatures of the pancreas, liver, and psoas major in the validation cohort. **c** The AUC for the radiomics signatures of the pancreas, liver, and psoas major in the prediction cohort. **d** The AUC for the filtered mean (Laplacian of Gaussian, sigma = 1.5) within pancreas ROI, original mean (without spatial filter process) within pancreas ROI, waist circumference, SAT, and VAT in the primary cohort. AUC, area under the curve; SAT, subcutaneous adipose tissue; VAT, visceral adipose tissue

had a C-index of 0.640 in the primary cohort and 0.697 in the validation cohort. The receiver-operating characteristic (ROC) curves for the radiomics signatures in the three cohorts are shown in Fig. 2. A representative image showing the diagnostic ability of the radiomics signature in the pancreas is shown in Fig. 3.

Prediction validation of the radiomics signature

The radiomics signature built from the features of the ROI in the pancreas yielded a C-index of 0.899 in the prediction cohort. In the model for the ROI in the liver, the radiomics signature only reached a C-index of 0.604 in the prediction cohort. The radiomics signature for the ROI in psoas major reached a C-index of 0.607 in the prediction cohort. Mindful that propensity score matching in validation and prediction cohorts could also be a confounding factor, we randomly selected another 147 control subjects with real distribution of patients (95 for the validation cohort and 52 for the prediction cohort, without matching process). The discriminatory power of the radiomics signature was comparable in the new cohorts to that in the matched cohorts. The C-index values for the radiomics signatures in the new cohorts are shown in Appendix Table 4. The characteristics of these new patients are listed in Appendix Tables 5 and 6.

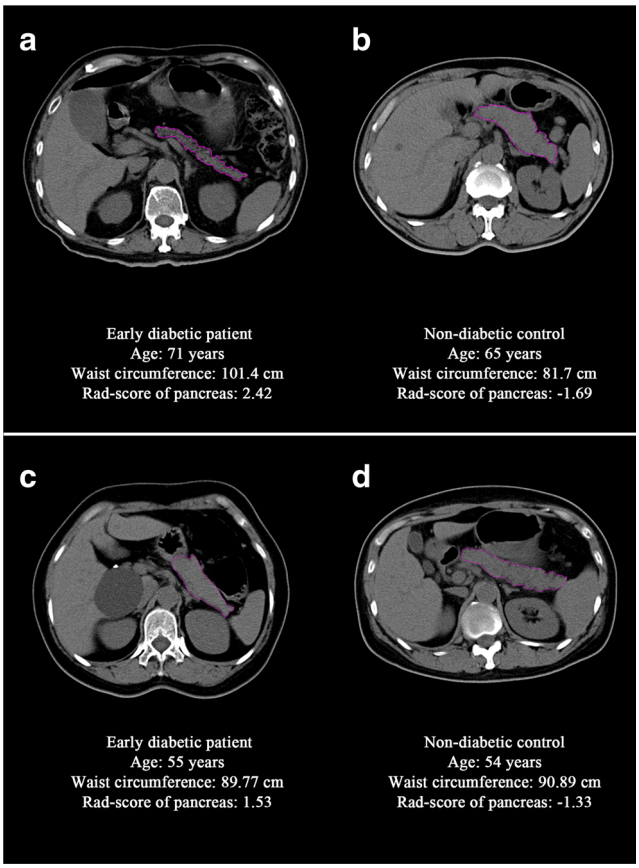

Fig. 3 Representative image of distinction between patients with early diabetes and non-diabetic controls using the radiomics score for the pancreas. **a** and **b** are CT images of a patient with early diabetes and a non-diabetic control with a large difference in the CT attenuation of the pancreas. **c** and **d** are images of another patient with early diabetes and a non-diabetic control in whom the CT attenuation of the pancreas does not show any apparent difference. However, the radiomics score for the pancreas can easily classify the early patients with diabetes and the non-diabetic controls in both situations. Note that Rad score of the pancreas can also recognize patients who were about to get diabetes. CT, computed tomography

Diagnostic and predictive value of the other markers

Only five of the 160 imaging features in the radiomics signature of the ROI in the pancreas remained as potential predictors. The discrimination performance of each feature was assessed after LASSO regression analysis (Appendix Table 7). We found that the mean of pancreas image filtered by a Laplacian of Gaussian spatial band-pass filter (mean_15_0, Appendix A3) had the highest discrimination accuracy. This single feature reached a C-index of 0.824, 0.822, and 0.911 in the primary cohort, validation cohort, and prediction cohort, respectively. We then tested the discriminatory power of the original mean CT value for the ROI in the pancreas without using the filtering process. The C-index of the mean CT value was only 0.695, 0.760, and 0.638 in the primary cohort, validation cohort, and prediction cohort, respectively (Table 3). The ROC curves for these two parameters and fat distribution parameters in the primary cohort were illustrated in Fig. 2d.

Development of an individualized diagnostic and prediction model

The radiomics signatures of the pancreas and liver were identified as independent predictors of a diagnosis of early diabetes after adjusting for the other predictors without imaging parameters (Table 4). A nomogram that incorporated the two predictors was developed and is shown in Fig. 4. The Hosmer-Lemeshow test yielded a nonsignificant statistic ($p = 0.273$), suggesting that there was no departure from a perfect fit. The C-index of the nomogram was 0.857 in the primary cohort.

The Hosmer-Lemeshow test yielded a nonsignificant statistic ($p = 0.243$ and $p = 0.923$ in the validation cohort and the prediction cohort, respectively), and the C-index of the nomogram was 0.878 in the validation cohort and 0.882 in the prediction cohort. The sensitivity and specificity of the nomogram reached 0.827 and 0.807 in the prediction cohort. Satisfactory calibration was observed in the three cohorts (Figure S3). The CT imaging parameters were added to the final logistic regression model for further analysis but had little impact on the discrimination performance (Appendix Table 8).

Table 3 Diagnostic characteristics of different predictors

Characteristic	Feature number	Selected features	Primary cohort		Validation cohort		Prediction cohort	
			C-index	95% CI	C-index	95% CI	C-index	95% CI
Radiomics signature								
Pancreas ROI	160	5	0.833	0.792–0.873	0.846	0.790–0.902	0.899	0.840–0.959
Liver ROI	160	9	0.697	0.646–0.748	0.687	0.612–0.761	0.604	0.495–0.712
Psoas Major ROI	160	8	0.640	0.586–0.695	0.697	0.623–0.771	0.607	0.499–0.714
Features of pancreas ROI								
Filtered mean (sigma = 1.5)	NA	NA	0.824	0.783–0.866	0.822	0.762–0.882	0.911	0.854–0.969
Original mean	NA	NA	0.695	0.624–0.746	0.760	0.702–0.810	0.638	0.530–0.746
Waist circumference	NA	NA	0.628	0.561–0.691	0.638	0.575–0.701	0.605	0.497–0.714
AAT	NA	NA	0.629	0.574–0.683	0.650	0.575–0.730	0.631	0.524–0.737
SAT	NA	NA	0.617	0.562–0.672	0.602	0.522–0.683	0.611	0.502–0.719
VAT	NA	NA	0.616	0.561–0.671	0.673	0.596–0.749	0.638	0.532–0.744

Original mean, mean CT attenuation within the ROI. Filtered mean, mean value within the ROI after the image had been filtered by spatial filters with different parameters

AAT area of abdominal adipose tissue, *CI* confidence interval, *ROI* region of interest, *SAT* area of subcutaneous abdominal adipose tissue, *VAT* area of visceral abdominal adipose tissue

Discussion

By comparing the results of three radiomics signatures based on different abdominal organs, we found that the radiomics signature of a ROI in the pancreas was most discriminant both for early diabetes screening and future diabetes prediction. We then developed and validated a radiomics signature–based nomogram for early diabetes screening and prediction of 3-year incident diabetes. The discriminatory power of the nomogram was slightly improved in the three cohorts. The nomogram also had an acceptable calibration so that the patients could be successfully stratified by the nomogram based on their risk of developing diabetes. To the best of our knowledge, this study is not only the first one to use a radiomics method to detect the development of type 2 diabetes but also the only study to predict future diabetes based on imaging.

A very optimistic discriminatory performance can be achieved using the mean value of the filtered image of pancreas. There were two reasons for the difference in intensity of the filtered image of pancreas between diabetic patients and the non-diabetic controls. Fatty infiltration not only lowered the CT attenuation but also blurred the texture features of the pancreas. Also, the contrast of the image of the pancreas between these two groups was greatly enhanced by the Laplacian filter, which highlights regions of rapid intensity change and is used for edge (texture) detection. Consequently, the difference in intensity between the fatty pancreas and normal pancreas was further enlarged. Without the image filtering process, the original mean value of the pancreas could only yield a low C-index in the three cohorts. Therefore, this study revealed that the changes in texture features in the pancreas were more sensitive than CT measurement of attenuation in a pre-diabetic or diabetic environment. Some imaging studies found that a fatty pancreas was associated with insulin resistance and β cell dysfunction [23–25]. Others conversely found that fat content of the pancreas was not related to either diabetes or insulin resistance [35, 36]. A high pancreatic fat content does not seem to be necessarily

Table 4 Risk Factors for diagnosis and prediction of early diabetes

Intercept and Variable	β	OR (95% CI)	*p* value
Intercept	-0.16	0.984	0.897
Radiomics signature of pancreas	1.342	3.828 (2.813–5.209)	< 0.001
Radiomics signature of liver	0.951	2.588 (1.679–3.900)	0.001
C-index			
Primary cohort		0.854 (0.816–0.891)	
Validation cohort		0.887 (0.839–0.936)	
Prediction cohort		0.884 (0.818–0.950)	

β is the regression coefficient. Only two radiomics signatures were incorporated in the model

CI confidence interval, *OR* odds ratio

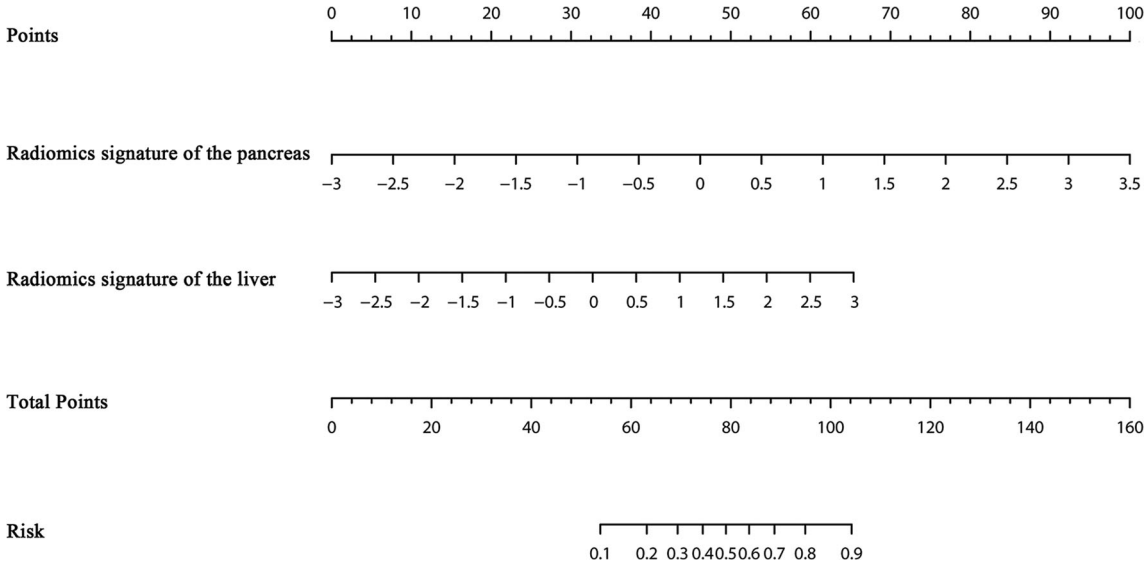

Fig. 4 The radiomics nomogram developed in this study. The radiomics nomogram incorporates the radiomics signature of the pancreas and the radiomics signature of the liver. By adding corresponding points for the two radiomics signatures (vertical projection to the first point scale), patients can be easily stratified according to their risk of developing diabetes (vertical projection from the total points scale to the risk scale)

associated to insulin resistance and β cell dysfunction. Meanwhile, there are also non-obese population who developed type 2 diabetes [37]. Some patients with normal weight were also enrolled in the early diabetic or pre-diabetic groups in our study. Hence, some structural changes reflected by radiomics signature in the pancreas of diabetic patients may also be independent of fat infiltration, and the radiomics signature may sever as a possible biomarker of incident diabetes in normal-weight individuals.

The liver and the skeletal muscle play a critical role in insulin resistance and glucose homeostasis [22]. Many studies, including some imaging investigations, have investigated the relationship between insulin resistance and ectopic accumulation of fat in the liver or skeletal muscle [38–42]. However, in our study, C-index values built from the ROIs in the liver and psoas major were lower than in the pancreas. Noteworthy, the predicting value of the liver signature was independent from that of the pancreas. One study also reported that liver fat was independent of β cell function in the pancreas in men with impaired glucose tolerance and type 2 diabetes [43]. The radiomics signature of the pancreas included only features of histogram, which mainly reflect the mean intensity of the coarse texture image (pancreas ROI image filtered by a Laplacian filter) of the pancreas, local and global intensity heterogeneity (standard deviation and kurtosis), while radiomics signature of liver comprised features of histogram and second-order statistical texture features (energy, correlation, and contrast, see Appendix A6). These results indicate different patterns of structural changes between the pancreas and liver during the development of diabetes. A rapid change of CT attenuation with perceptible edges in the pancreas image and a subtle change of the texture of the liver parenchyma suggest the structural alteration might be more macroscopic and sporadic in the pancreas, while is smaller in scale and more widespread in the liver.

Fat distribution parameters, including areas of AAT, VAT, SAT, and the VAT/SAT ratio, were also investigated in this study. However, we found that these measurements alone might not be sufficient for clinical use. Radiomics investigates fat distribution at the microscopic level, outperforming the macroscopic evaluation of fat distribution. A recent study used CT attenuation to indirectly reflect the cellular characteristics of adipose tissue and found that a high SAT density was related to an increased risk of diabetes [44]. It would be also possible to use radiomics methods to investigate AAT in metabolic disease.

This study has several limitations. Firstly, the subjects enrolled in the study were all inpatients at our institution. The sick condition of the patients may have been a confounding factor in the analysis. We attempted to analyze the difference of the disease composition of patients and found that there was no difference among the three groups with this regard (Figure S5). Secondly, the sample size for the pre-diabetic patients was too small. Thirdly, the study protocol was data-driven, such that the radiomics model used was more similar to a diagnostic model than a predictive one.

In conclusion, this study presents a radiomics model based on texture analysis of subtle structural changes within the abdominal organs, mainly the pancreas. It could be used to screen for early diabetes and predict 3-year incident diabetes. The good discriminatory power of this method highlights the existence of early pathological structural changes in abdominal organs during the development of diabetes. Future developments may occur in three directions: MRI, given superior

soft-tissue contrast and higher resolution compared to CT, might provide even better results; 3D segmentation may give a more comprehensive evaluation of subtle structural changes when combined with radiomics method, if robust and accurate automated 3D segmentation algorithms are developed; larger and multi-centric studies, prospective or retrospective, are required to validate the role of radiomics in the prediction and assessment of metabolic diseases.

Acknowledgements The authors acknowledge the technical assistance of Professor Shou-Hua Luo from the Image and Signal Processing Laboratory at the Southeast University.

Funding This study has received funding by the National Nature Science Foundation of China (NSFC, No. 81525014), the Jiangsu Provincial Special Program of Medical Science (BL2013029), and the Key Research and Development Program of Jiangsu Province (BE2016782).

Compliance with ethical standards

Guarantor The scientific guarantor of this publication is Shenghong Ju.

Conflict of interest The authors declare that they have no conflict of interest.

Statistics and biometry No complex statistical methods were necessary for this paper.

Informed consent Written informed consent was waived by the Institutional Review Board.

Ethical approval Institutional Review Board approval was obtained.

Methodology
- Retrospective
- Diagnostic or prognostic study
- Performed at one institution

References

1. NCD Risk Factor Collaboration (NCD-RisC) (2016) Worldwide trends in diabetes since 1980: a pooled analysis of 751 population-based studies with 4. 4 million participants. Lancet 387:1513–1530
2. Guo F, Garvey WT (2015) Development of a weighted cardiometabolic disease staging (CMDS) system for the prediction of future diabetes. J Clin Endocrinol Metab 100:3871–3877
3. Diabetes Prevention Program Research Group, Knowler WC, Fowler SE et al (2009) 10-year follow-up of diabetes incidence and weight loss in the diabetes prevention program outcomes study. Lancet 374:1677–1686
4. Beagley J, Guariguata L, Weil C, Motala AA (2014) Global estimates of undiagnosed diabetes in adults. Diabetes Res Clin Pract 103:150–160
5. Fisher-Hoch SP, Vatcheva KP, Rahbar MH, McCormick JB (2015) Undiagnosed diabetes and pre-diabetes in health disparities. PLoS One 10:e0133135
6. Lee YH, Armstrong EJ, Kim G et al (2015) Undiagnosed diabetes is prevalent in younger adults and associated with a higher risk cardiometabolic profile compared to diagnosed diabetes. Am Heart J 170:760–769 e762
7. Zhou X, Qiao Q, Ji L et al (2013) Nonlaboratory-based risk assessment algorithm for undiagnosed type 2 diabetes developed on a nation-wide diabetes survey. Diabetes Care 36:3944–3952
8. Ding D, Chong S, Jalaludin B, Comino E, Bauman AE (2015) Risk factors of incident type 2-diabetes mellitus over a 3-year follow-up: results from a large Australian sample. Diabetes Res Clin Pract 108: 306–315
9. Abbasi A, Sahlqvist AS, Lotta L et al (2016) A systematic review of biomarkers and risk of incident type 2 diabetes: an overview of epidemiological, prediction and aetiological research literature. PLoS One 11:e0163721
10. Kengne AP, Beulens JW, Peelen LM et al (2014) Non-invasive risk scores for prediction of type 2 diabetes (EPIC-InterAct): a validation of existing models. Lancet Diabetes Endocrinol 2:19–29
11. Herder C, Kowall B, Tabak AG, Rathmann W (2014) The potential of novel biomarkers to improve risk prediction of type 2 diabetes. Diabetologia 57:16–29
12. Grundy SM (2012) Pre-diabetes, metabolic syndrome, and cardiovascular risk. J Am Coll Cardiol 59:635–643
13. Wang A, Chen G, Su Z et al (2016) Risk scores for predicting incidence of type 2 diabetes in the Chinese population: the Kailuan prospective study. Sci Rep 6:26548
14. Abbasi A, Peelen LM, Corpeleijn E et al (2012) Prediction models for risk of developing type 2 diabetes: systematic literature search and independent external validation study. BMJ 345:e5900
15. Chiu HK, Tsai EC, Juneja R et al (2007) Equivalent insulin resistance in latent autoimmune diabetes in adults (LADA) and type 2 diabetic patients. Diabetes Res Clin Pract 77:237–244
16. McTernan CL, McTernan PG, Harte AL, Levick PL, Barnett AH, Kumar S (2002) Resistin, central obesity, and type 2 diabetes. Lancet 359:46–47
17. Kaess BM, Pedley A, Massaro JM, Murabito J, Hoffmann U, Fox CS (2012) The ratio of visceral to subcutaneous fat, a metric of body fat distribution, is a unique correlate of cardiometabolic risk. Diabetologia 55:2622–2630
18. Tang L, Zhang F, Tong N (2016) The association of visceral adipose tissue and subcutaneous adipose tissue with metabolic risk factors in a large population of Chinese adults. Clin Endocrinol (Oxf) 85: 46–53
19. Storz C, Heber SD, Rospleszcz S et al (2018) The role of visceral and subcutaneous adipose tissue measurements and their ratio by magnetic resonance imaging in subjects with prediabetes, diabetes and healthy controls from a general population without cardiovascular disease. Br J Radiol. https://doi.org/10.1259/bjr.20170808: 20170808
20. Liu L, Feng J, Zhang G et al (2018) Visceral adipose tissue is more strongly associated with insulin resistance than subcutaneous adipose tissue in Chinese subjects with pre-diabetes. Curr Med Res Opin 34:123–129
21. Onat A, Uğur M, Can G, Yüksel H, Hergenç G (2010) Visceral adipose tissue and body fat mass: predictive values for and role of gender in cardiometabolic risk among Turks. Nutrition 26:382–389
22. Shulman GI (2014) Ectopic fat in insulin resistance, dyslipidemia, and cardiometabolic disease. N Engl J Med 371:2237–2238
23. Wong VW, Wong GL, Yeung DK et al (2014) Fatty pancreas, insulin resistance, and beta-cell function: a population study using fat-water magnetic resonance imaging. Am J Gastroenterol 109: 589–597
24. Tushuizen ME, Bunck MC, Pouwels PJ et al (2007) Pancreatic fat content and beta-cell function in men with and without type 2 diabetes. Diabetes Care 30:2916–2921

25. Aerts HJ, Velazquez ER, Leijenaar RT et al (2014) Decoding tumour phenotype by noninvasive imaging using a quantitative radiomics approach. Nat Commun 5:4006
26. Gillies RJ, Kinahan PE, Hricak H (2016) Radiomics: images are more than pictures, they are data. Radiology 278:563–577
27. Lambin P, Rios-Velazquez E, Leijenaar R et al (2012) Radiomics: extracting more information from medical images using advanced feature analysis. Eur J Cancer 48:441–446
28. Liu Z, Zhang XY, Shi YJ et al (2017) Radiomics analysis for evaluation of pathological complete response to neoadjuvant chemoradiotherapy in locally advanced rectal cancer. Clin Cancer Res. https://doi.org/10.1158/1078-0432.CCR-17-1038:clincanres.1038.2017
29. Huang YQ, Liang CH, He L et al (2016) Development and validation of a radiomics nomogram for preoperative prediction of lymph node metastasis in colorectal cancer. J Clin Oncol 34:2157–2164
30. Kuo MD, Jamshidi N (2014) Behind the numbers: decoding molecular phenotypes with radiogenomics–guiding principles and technical considerations. Radiology 270:320–325
31. McDonald RJ, McDonald JS, Kallmes DF, Carter RE (2013) Behind the numbers: propensity score analysis-a primer for the diagnostic radiologist. Radiology 269:640–645
32. Shafiq-Ul-Hassan M, Zhang GG, Latifi K et al (2017) Intrinsic dependencies of CT radiomic features on voxel size and number of gray levels. Med Phys 44:1050–1062
33. He L, Huang Y, Ma Z, Liang C, Liang C, Liu Z (2016) Effects of contrast-enhancement, reconstruction slice thickness and convolution kernel on the diagnostic performance of radiomics signature in solitary pulmonary nodule. Sci Rep 6:34921
34. Harrell FE Jr, Lee KL, Mark DB (1996) Multivariable prognostic models: issues in developing models, evaluating assumptions and adequacy, and measuring and reducing errors. Stat Med 15:361–387
35. Kühn JP, Berthold F, Mayerle J et al (2015) Pancreatic steatosis demonstrated at MR imaging in the general population: clinical relevance. Radiology 276:129–136
36. Nowotny B, Kahl S, Kluppelholz B et al (2018) Circulating triacylglycerols but not pancreatic fat associate with insulin secretion in healthy humans. Metabolism 81:113–125
37. Vaag A, Lund SS (2007) Non-obese patients with type 2 diabetes and prediabetic subjects: distinct phenotypes requiring special diabetes treatment and (or) prevention? Appl Physiol Nutr Metab 32:912–920
38. Perry RJ, Samuel VT, Petersen KF, Shulman GI (2014) The role of hepatic lipids in hepatic insulin resistance and type 2 diabetes. Nature 510:84–91
39. Awazawa M, Gabel P, Tsaousidou E et al (2017) A microRNA screen reveals that elevated hepatic ectodysplasin A expression contributes to obesity-induced insulin resistance in skeletal muscle. Nat Med 23:1466–1473
40. Camastra S, Vitali A, Anselmino M et al (2017) Muscle and adipose tissue morphology, insulin sensitivity and beta-cell function in diabetic and nondiabetic obese patients: effects of bariatric surgery. Sci Rep 7:9007
41. Bril F, Barb D, Portillo-Sanchez P et al (2017) Metabolic and histological implications of intrahepatic triglyceride content in nonalcoholic fatty liver disease. Hepatology 65:1132–1144
42. Cusi K, Sanyal AJ, Zhang S et al (2017) Non-alcoholic fatty liver disease (NAFLD) prevalence and its metabolic associations in patients with type 1 diabetes and type 2 diabetes. Diabetes Obes Metab 19:1630–1634
43. Tushuizen ME, Bunck MC, Pouwels PJ, Bontemps S, Mari A, Diamant M (2008) Lack of association of liver fat with model parameters of beta-cell function in men with impaired glucose tolerance and type 2 diabetes. Eur J Endocrinol 159:251–257
44. Yeoh AJ, Pedley A, Rosenquist KJ, Hoffmann U, Fox CS (2015) The association between subcutaneous fat density and the propensity to store fat viscerally. J Clin Endocrinol Metab 100:E1056–E1064